Pore Size Distribution Analysis of Structure Different Microporous Carbons – Theoretical Evaluation Based on Density Functional Theory and Nitrogen and Argon Experimental Adsorption Isotherms at 77 K

P. Kluson and S. J. Scaife*

Faculty of Chemical Technology, Institute of Chemical Technology, Technicka 5, 166 28 Prague 6, Czech Republic, e-mail: P.Kluson@seznam.cz

*Department of Chemistry, University of Wales in Bangor, Gwynedd LL57 2UW, North Wales, United Kingdom

Original scientific paper
Received: 15. 1. 2001.
Accepted: 1. 4. 2001.

Nitrogen and argon adsorption isotherms on four significantly different microporous carbons were experimentally measured at 77K. Non-local density functional theory was used to predict theoretically the behaviour of both gases in slit-shaped pores in adsorption. Adsorbate molecules were modelled as spheres, fluid-fluid and solid-fluid interactions were described by 12–6 Lennard-Jones and 10–4–3 Steele potentials, respectively. Potential parameters were obtained by fitting the calculated data to experimental isotherms of nitrogen and argon on a non-microporous carbon surface. These results were used for the theoretical evaluation of pore size distribution. An algorithm for the pore size distribution analysis from adsorption data (theoretical and experimental) was suggested and tested on the adsorption data obtained.

Keywords:

Density functional theory, pore size distribution, adsorption of nitrogen, adsorption of argon, microporous carbons.

Introduction

Activated carbons or charcoal are important modifications of carbon prepared by carbonisation and activation of various raw materials in several consecutive[1] steps. This procedure creates a high specific surface area by oxidative generation of micropores of variable size and shape distribution depending upon the raw material used and process conditions (temperature, activation agents, etc.). The source of carbons relevant to the present context is a feedstock of small hydrocarbon molecules (aliphatic or aromatic) and various[1,2] biopolymers.

Microporous carbons are used as prominent adsorbents in a vast range of industrial processes,[3] in waste water treatment, in purification of exhaust gases of various origin and also[4] as superior catalytic supports. This multiple role operates in parallel with their complex structural chemistry. The typical activated carbon[1,2,5] is a network of interconnected pores of graphitic nature. Its complicated structure differs from sample to sample and cannot be described by experiments alone. However, it also cannot be realistically modelled without making assumptions such as: the slit-pore geometry, negligible pore-junction effects and a complete absence of functional groups and surface defects.[5–11]

Statistical mechanics methods in gas adsorption[8,12–23] allow what one can never observe experimentally, that is how adsorption isotherms change with varying pore size. A set of local isotherms theoretically generated for adsorption of two different gases inside of pores of particular size could be directly used[8,12,14,15] for prediction of adsorption selectivity. Consequently, a set of separation factors (selectivities) evaluated for a particular pore size range gives the potential to design completely a microporous structure of a desired carbonaceous adsorbent for a studied process. To such a surface[8,12] a real adsorbent with known PSD (pore size distribution) could be assigned. Availability of a database of commercial microporous carbons characterised by their PSD patterns is of immense importance. Consequently, there is an urgent need for a standard, reliable method competent to evaluate pore size distributions of such carbons from simple adsorption data. Typically, either nitrogen or argon adsorption at 77K offer[4,24–26] a convenient characterisation tool. Empirical or semi-empirical methods for PSD analysis do not assume contribution of individual pores and are virtually based on macroscopic features of adsorption isotherms[e.g.4,24,27–31] and often do not predict PSD correctly. On the other hand GCMC (Grand Canonical Monte Carlo) or NL-DFT (Non-local Density Functional Theory) methods[5,32–36] are the tools that statistical mechanics

*The author to whom a correspondence should be addressed

offers for interpretation of PSD through experimental adsorption isothermal data.

In this paper we report on nitrogen and argon adsorption experiments at 77K and on pore size distribution analysis of four significantly different microporous carbons AX21, PICA, Norit and Supersorbon by using non-local density functional theory for prediction of behaviour of nitrogen and argon in adsorption in slit-like pore geometry. Both the nitrogen and argon molecules were modelled as single centred spheres without quadrupole or partial charges. The gas-solid potential parameters were obtained by fitting the calculated adsorption isotherm of a single model adsorbent surface (H* = 100) to the experimental data on non-microporous carbon Vulcan. The graphitised carbon Vulcan, widely used for evaluation of potential parameters in theoretical modeling of adsorption and as a basis for prediction of pore size distribution, already represents a fairly good approximation of a flat and regular graphite surface. The main intention of this study was to present a reliable theoretical method for evaluation of PSD of microporous carbons from nitrogen and argon adsorption isotherms. Extension of this work focused on pore size distribution analysis[37] from adsorption data of a wider range of gases (methane, carbon dioxide, nitrogen, argon) at different temperatures was presented recently. The work focused on the comparison of the presented approach with standard methods (such as DR analysis) is being currently prepared and will be a subject of one of our future communications.

Experimental

Experimental part

Adsorbents

Certified reference material – low surface area graphitised carbon black No. M11–02 (Vulcan 3-G)[38] supplied by Laboratory of the Government Chemists and microporous carbons AX21 (MAST),[25] Supersorbon HB-3 (Degussa), Norit R-0.8/53833 (Norit N.V.), PICA (AirLiquide) were used as adsorbents.

SEM

Surface images of the four carbons were taken on a SEM apparatus (Hitachi S-520) at U = 14kV. Samples were fixed on a microscopy holder by a conductive carbon tape and sputtered with gold in plasma.

Adsorbates

Nitrogen – high purity gas (99.999 %) supplied by Air Products.

Argon – high purity gas (99.999 %) supplied by Air Products.

Helium („dead space" calibration) – high purity gas (99.9 %) supplied by Air Products.

Experimental equipment and experimental conditions

The volumetric adsorption experiments were conducted on Omnisorp 100CX (Coulter) at 77 K in a static regime. Each sample was outgassed under high vacuum (10^{-5} Torr) before a measurement (523 K for 10 hr – Vulcan, 573 K for 16 hr – microporous carbons). The volume of gas adsorbed was determined as a function of the bulk gas pressure. The dead space volume was measured with helium under experimental conditions.

Modelling of adsorption

Adsorbent model

The microporous surface was approximated by a homogeneous potential function as an assembly of close-packed atoms each of which is characterised by the potential parameters ε and σ. In the slit pore model[21,39,40] used the pore consists of two parallel graphitic slabs. The distance between the nuclei of the carbon atoms on each opposing slab is defined as the physical pore width, H_{phys}. The influence of connectivity in the pore was neglected by the assumption that the ratio of pore length to pore width is large.

Adsorbate models

Adsorbates molecules were modelled as single centred LJ hard spheres. The interaction between two adsorbate molecules[12–15,24,25,40–43] is described by the Lennard-Jones (12–6) pair potential:

$$\phi_{ff}(r) = 4\ \varepsilon_{ff}\ [(\sigma_{ff} / r)^{12} - (\sigma_{ff} / r)^{6}] \qquad (1)$$

where r is the separation distance between two fluid atoms and ε_{ff} and σ_{ff} are fitted parameters for the bulk adsorbate well-depth and molecular diameter respectively. The interaction potential for the adsorbate interacting with a single graphite slab is described[8,13–15,25,26] by the Steele 10–4–3 potential.

$$\phi_{sf}(z) = \varepsilon_{w}\ \{2/5(\sigma_{sf}/z)^{10} - (\sigma_{sf}/z)^{4} - (\sigma_{sf}^{4}/3\Delta(z + 0.6\Delta)^{3}\} \qquad (2)$$

where z is the distance from the graphite surface, σ_{sf} is the effective adsorbate-adsorbent (carbon) intermolecular diameter, Δ is the separation between graphite layers and ε_{w} is given by:

$$\varepsilon_{w} = 2\ \Pi\ \varepsilon_{sf} \rho_{s}\ \sigma_{sf}^{2}\ \Delta \qquad (3)$$

where ρ_s is the number of carbon atoms per unit volume in graphite (114 nm^{-3}), and ε_{sf} is the parameter for the adsorbate-carbon interaction potential well-depth. The solid-fluid parameters were calculated by combining the graphite parameters with the appropriate fluid parameters using the Lorentz-Berthelot mixing rules.[13–15,25,26] The Steele potential describes interactions between the adsorbate molecule and one graphite slab, however, in a slit-pore geometry the adsorbate molecule will interact with two pore walls and hence the potential is written as:

$$V_{ext}(z) = \phi_{sf}(z) + \phi_{sf}(H - z) \quad (4)$$

The potential parameter values for nitrogen and argon were estimated by fitting the theoretical adsorption isotherms of a large pore ($H^* = 100$), which represents a flat surface, to the experimental isotherm of graphitised carbon Vulcan.

Details of the DFT method are given[5,25,26,43,44] elsewhere.

Determination of PSD

The experimental adsorption isotherm measured is approximated[25,26,45] as an adsorption integral function:

$$N(P) = \int_{H_{min}}^{H_{max}} \rho(P,H)\, f(H)\, dH \quad (5)$$

where $N(P)$ represents the experimental isotherm and $\rho(P, H)$ is a local isotherm calculated from NL-DFT. The $f(H)$ is non-negative and is normalised to unity.

$$\int_{H_{min}}^{H_{max}} f(H)\, dH = 1 \quad (6)$$

Once $\rho(P, H)$ and $N(P)$ are known, the equation (5) is solved for $f(H)$. The solution is a multi-modal gamma distribution function given by the expression:

$$f(H) = \sum_{i=1}^{m} (\alpha_i (\gamma_i H)^{\beta i}) / (\Gamma(\beta_i) H) \exp(-\gamma_i H) \quad (7)$$

where m is the number of modes in the distribution, H is a pore width, α_i, β_i and γ_i are adjustable parameters related to the amplitude, mean and variance of mode i, respectively. The number of modes in this equation is equal to the number of inflection points on the experimental adsorption isotherm $N(P)$. Initial starting values are assigned to the parameters α_i, β_i and γ_i, which constrain $f(H)$. The solution that is considered to be $f(H)$ is the one that gives the best fit to the experimentally determined total isotherm. In this work it is obtained numerically by minimising the sum of the square of the differences E, between the experimental and theoretical isotherms:

$$E = 1/n_P \sum_{i=1}^{n_P} \left[\sum_{i=1}^{n_H} \rho(P_i, H_j) f(H_j) \Delta H_j - N(P_i) \right]^2 \quad (8)$$

where E is the mean square error per a fitted point, n_P is the number of experimental points, and n_H is the total number of pore widths.

Results and discussion

AX21, Supersorbon, PICA and Norit microporous carbons were chosen as model surfaces from a wide selection of commercially available adsorbents. Micrographs of their surfaces are shown in Figures 1, 2, 3 and 4. The surface of AX21 (Figure 1) looks quite homogeneous with fractures typical for this kind of a material and it is similar to that of Norit (Figure 2). Supersorbon is composed from many flat sheets as it could be recognised inside of an „abyss" in Figure 3. A completely different surface structure is exhibited by PICA. At lower magnification the step like surface could be observed, at higher magnification a surface composed of lappets appears (Figure 4a,b).

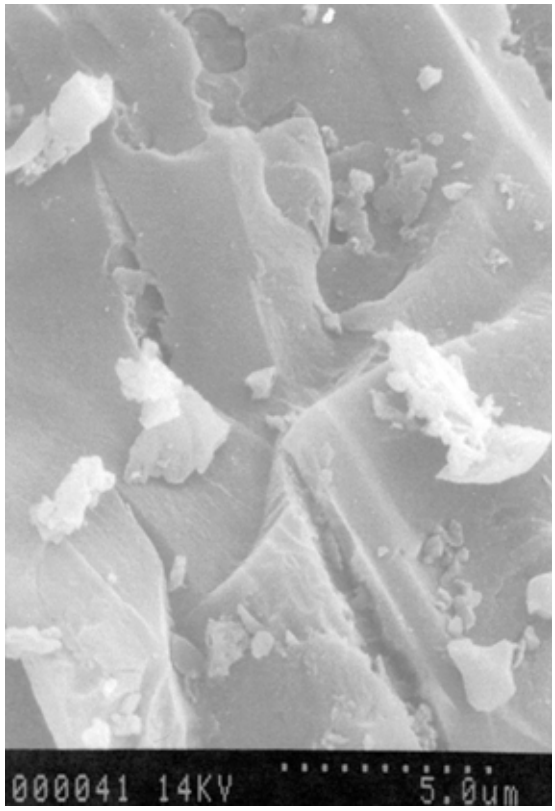

Fig. 1 – *SEM image of the surface of AX21*

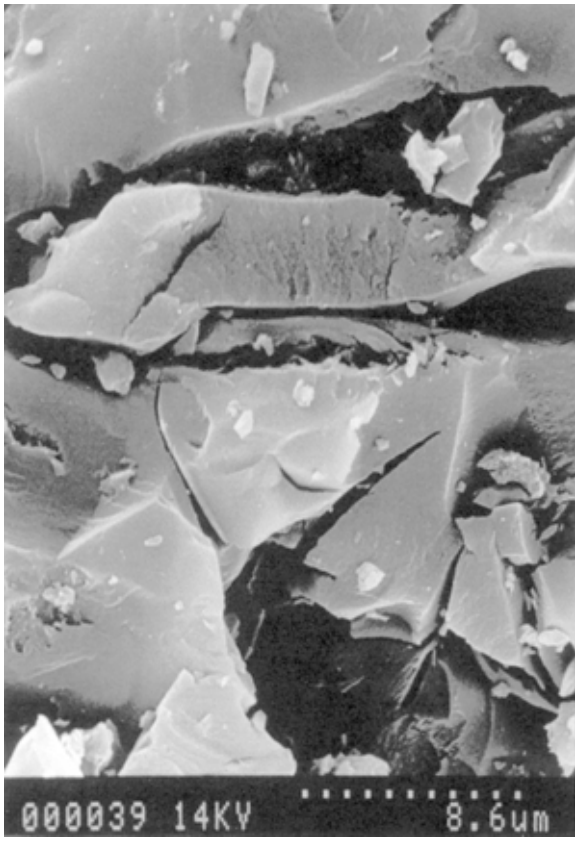

Fig. 2 – *SEM image of the surface of Norit*

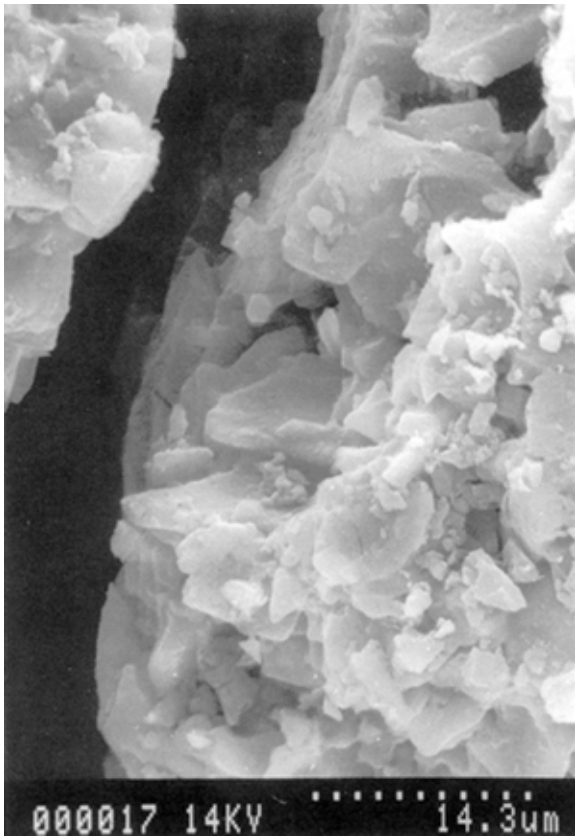

Fig. 3 – *SEM image of the surface of Supersorbon*

a)

b)

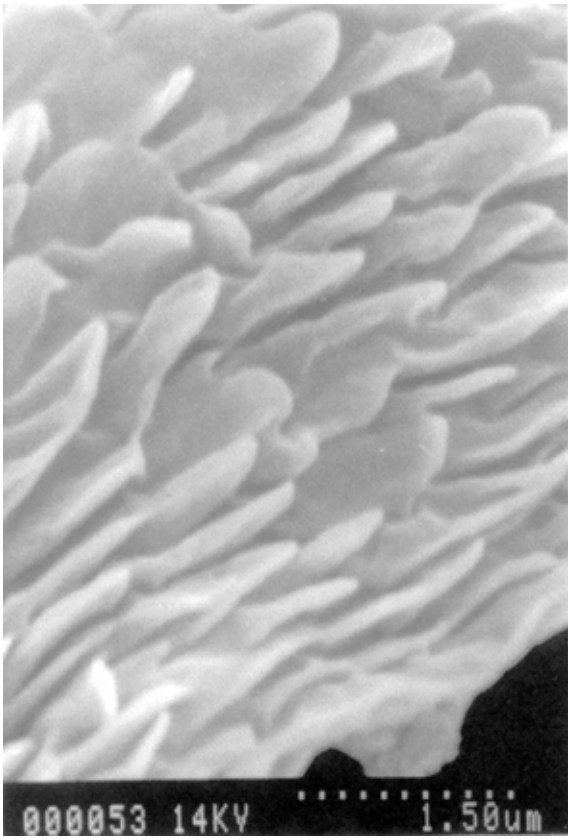

Fig. 4a,b – *SEM images of the surface of PICA*

These four carbons were chosen mainly because of their distinctively different adsorption properties. Experimental nitrogen isotherms are shown in Figure 5 up to the relative pressure of $P/P_o = 1$. It is seen that the activated carbons differ significantly in monolayer capacities, monolayer completion pressures, layering transitions gradients and in the overall adsorption capacities. Such differences comply with the main intention of this study, that is to present a reliable method for PSD analysis capable of description of porous structures of different carbonaceous surfaces. Adsorption isotherms on the surface of AX21 exhibit the formation of two distinctive layers, which is also a common feature of all studied carbons. The initial uptake of nitrogen at very low pressures is largest for AX21, the other three isotherms are comparable in this region. Despite the different volumes of gas adsorbed, which correspond to the different contributions of narrow pores (different pore volumes), the presence of very narrow pores (less than H = 1nm) is a common property of all the adsorbates since adsorption isotherms start at comparatively similar relative pressure values. Above this region there is a zone in the middle of which points of inflections are located. This part corresponds to the saturation of edges and other inhomogeneous sites on the surface and it precedes a monolayer formation. In this region distinctions between Norit and Supersorbon and PICA are already pronounced, however, the course of adsorption on the latter two is still similar up to the inflection point. The monolayer completion is generally located around $P/P_o = 0.0005$, however, it is not well pronounced for AX21. Layering transitions from the first to the second layer is quite steep for AX21; Supersorbon and Norit show moderate gradient and the second layer formation region on PICA is rather flat. The total adsorption capacity at the relative pressure of $P/P_o = 1$ is highest for AX21, followed by Supersorbon, which is in turn higher than the already similar values for Norit and PICA.

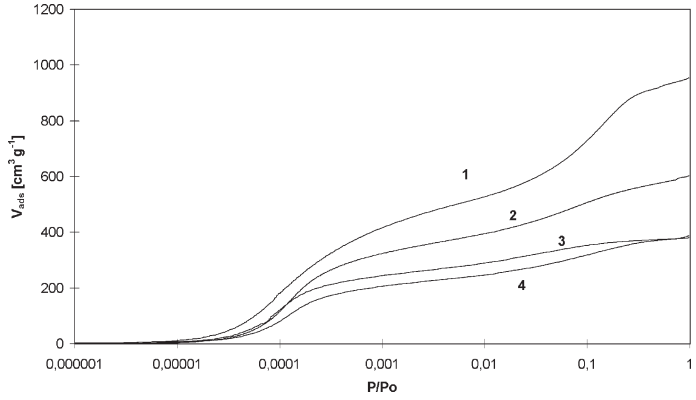

F i g . 5 – *Nitrogen adsorption isotherms on AX21(1), Supersorbon (2), PICA (3) and Norit (4)*

Isotherms determined with different adsorbates usually vary for the same adsorbent as these surface probe molecules exhibit quite different condensation properties, molecular size, shape and other corresponding parameters. Adsorption of nitrogen on AX21 and Supersorbon was compared with argon adsorption data under the same conditions to extend a list of isotherms on which the proposed PSD evaluation method would be tested. The isotherms are plotted in Figure 6 together with corresponding curves for nitrogen. Both the argon isotherms are roughly similar in shape to their counterparts from nitrogen adsorption and thus a similar discussion also applies. The main differences comprise of a much larger initial nitrogen uptake, which is soon followed by a steeper uptake of argon. There is also a difference in the location of regions (relative pressure axis), in which the curves approach closely to each other. Consequently an intersection of argon and nitrogen isotherms must appear at significantly different positions for each of them (at $P/P_o = 0.001$ for Supersorbon and $P/P_o = 0.01$ for AX21). Argon adsorbed on AX21 is even less willing to form a distinctive monolayer than nitrogen, however, the second layer is well developed. This behaviour is reversed on the surface of Supersorbon: well developed the first layer, much flatter the second layer and difficult to determine completion of adsorption.

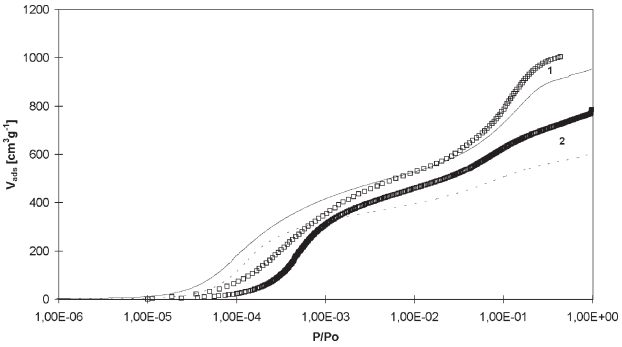

F i g . 6 – *Adsorption of argon (□) and nitrogen (solid line) on AX21 (group 1) and Supersorbon (group2)*

In agreement with other authors[46–48] we did not observe any indication of solidification of argon in narrow pores at 77K (subcritical to argon). A freezing point depression is probably the reason, however, even on the surface of non-microporous carbon no dramatic differences between adsorption of argon at 77K and 87K (its critical temperature) were observed.

Adsorption of nitrogen and argon was also experimentally studied on the surface of non-microporous graphitised carbon black Vulcan. To its wide pores, theoretical isotherms generated by NL-DFT were fitted with the intention of obtaining potential

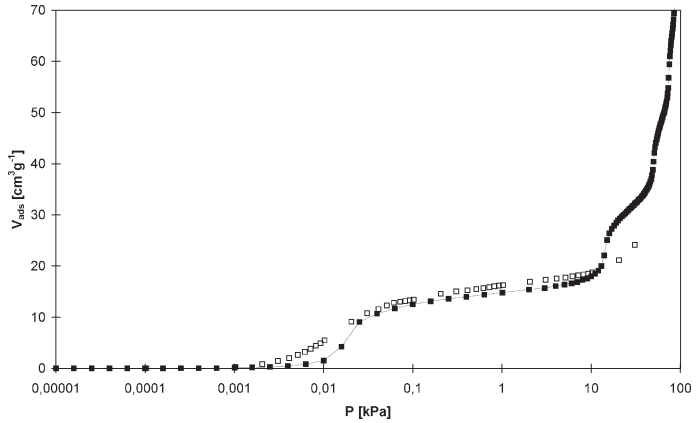

Fig. 7 – *Adsorption of nitrogen on Vulcan; (□) – experimental isotherm, (■) – dft fit*

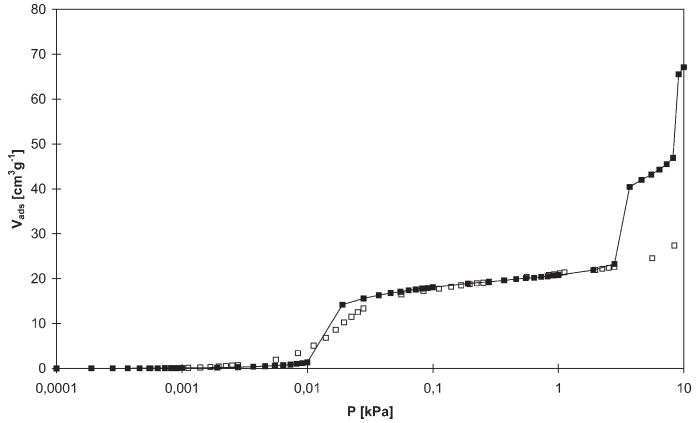

Fig. 8 – *Adsorption of argon on Vulcan; (□) – experimental isotherm, (■) – dft fit*

parameters for generation of local isotherms. Figures 7 and 8 show experimental nitrogen and argon isotherms and their fitted theoretical counterparts. For the fitting procedure it is of great importance to choose a region of the isotherm that is most representative of the solid-fluid interactions. Interfering fluid-fluid forces are minimised by the adsorbed density at low pressures. In the pore size distribution analysis the solid-fluid potential strength influences the filling pressures of micropores strongly and thus it is essential that this parameter is carefully fitted particularly inside of the low pressure region. For the calculated[49] potential parameters listed in Table 1 there is typically a low pressure region, where DFT underpredicts the course of adsorption, whilst at high pressure it overpredicts it. Although there is a good chance to improve the fit partially, it is always accompanied by losing a quality of the fit in other regions. Quality of the fit obtained was better for nitrogen (Figure 7) than for argon (Figure 8). The model for argon gives very sharp transition. The differences between experimental and theoretical isotherms found are generally due to either the model of the carbon surface (a

Table 1 – *Fluid-fluid and solid-fluid potential parameters*

Parameter	Nitrogen	Argon
σ_{ff} (nm)	0.3572	0.3410
σ_{sf} (nm)	0.3486	0.3405
ε_{ff}/k (K)	93.98	119.8
ε_{sf}/k (K)	53.46	54.86

smooth surface was modelled, while the real experimental surface is never perfectly smooth), the adsorbate model (e.g., quadrupole is not included for nitrogen), or the DFT theory itself. Detail discussion is given elsewhere.[49]

In order to solve the equation (5) for f(H) a minimisation algorithm which uses equation (8) was employed. When E converged to a minimum value the best fit to the experimental adsorption was attained and consequently the pore size distribution was calculated. As an example, a theoretical fit to nitrogen experimental isotherm up to the pressure of 10 kPa on AX21 is presented in Figure 9. The quality of fits achieved were generally similarly good for all surfaces studied.

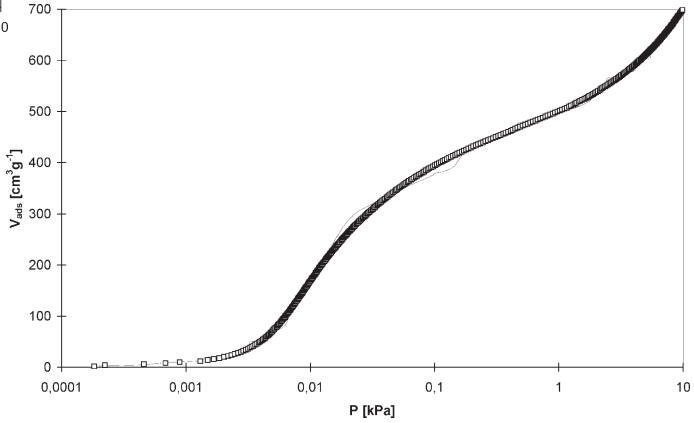

Fig. 9 – *Nitrogen experimental isotherm on AX21 (□) and its dft fit (solid line)*

Pore size distribution patterns of AX21, Supersorbon, PICA and Norit evaluated from the nitrogen theoretical database and corresponding experimental data are shown in Figure 10. A bimodal distribution is well developed for AX21 only. The second maximum for the three other carbons is rather low, nevertheless for Norit and Supersorbon it is still well defined. PICA's second peak is almost flat, thus it's PSDs pattern could be referred to as practically unimodal. PSDs of AX21 and Supersorbon show a significant contribution of ultra-narrow pores of size less than H = 1 nm. The region between H = 1 nm to H = 1.7 nm is the most repre-

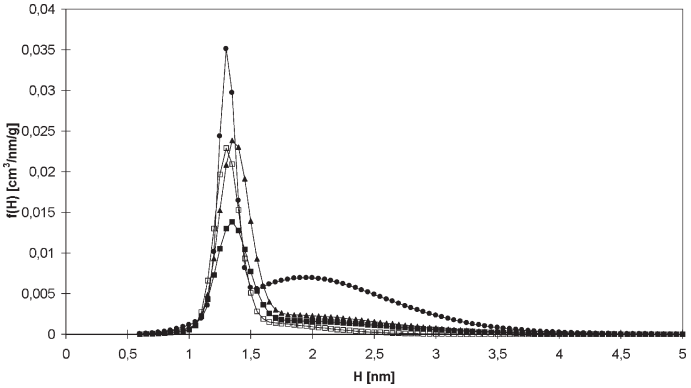

Fig. 10 – *PSD patterns of AX21 (●), Supersorbon (▲), PICA (□) and Norit (■) from nitrogen adsorption*

sentative pore size interval of all the carbons. The highest first peak was found for AX21 followed by Supersorbon, PICA, and Norit. The first peaks for AX21 and PICA are somewhat narrower compared with those of Supersorbon and Norit. This behaviour corresponds with characteristic features of their nitrogen isotherms. The second maximum of AX21 covers a region of H = 1.5 nm to H = 5 nm, above this limit no substantial contribution to adsorption was observed. The second peak has its maximum at about H = 2nm, the maxima of Supersorbon and Norit peak approximately at the same position. The second missing peak on PICA's PSD pattern corresponds well to it's very flat region in which a second layer was formed. The points of inflection after the monolayer formation and consequently the second layers are much more pronounced on Norit and Supersorbon adsorption curves. The second layer on AX21 is very distinctive which is reflected in a considerable contribution of mesopores to the adsorption (the second maximum on the PSD curve).

Pore size distributions of AX21 and Supersorbon evaluated from argon database and argon experimental isotherms are given in Figure 11. In this case both the patterns are bimodal with distinctive second maxima covering the mesoporous region. The first peak of AX21 distribution is less sharp than that of Supersorbon, however, it covers a substantial contribution of ultra narrow pores (less than H = 1nm). According to this and in agreement with the argon experimental isotherms, Supersorbon contains less ultra-narrow pores than AX21. It again complies well with the much steeper uptake of argon after the very low pressure region and formation of a distinct point of inflection (Supersorbon). The second peak covering the mesoporous structure of both of the materials is higher for AX21, which corresponds to a more pronounced second layer than that observed on Supersorbon.

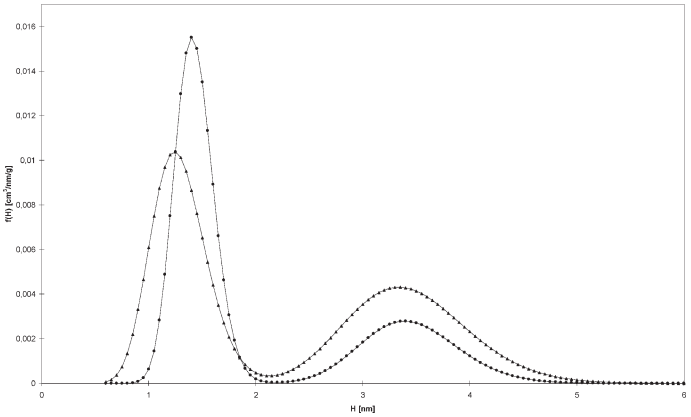

Fig. 11 – *PSD patterns of AX21 (●) and Supersorbon (▲) from argon adsorption*

The sensitivity of the pore size distribution to the extent of data in the database was also studied. The database containing 63 isotherms ranging from H = 0.6 nm to H = 100 nm, with an incremental increase in physical pore width of 0.1 nm was used in conjunction with experimental data for the adsorption of nitrogen on AX21. The resulting PSD(1) in Figure 12 is identical with that one already given in Figure 10. According to the figure, AX21 consists of pores ranging from H = 0.6 nm to H = 5 nm and the location of the peak maxima indicates the greatest proportion of slit pores with widths of around 1.3 nm and 2.1 nm. The database was then reduced by increasing the step size in physical pore width to 0.2 nm. The PSD(2) obtained is also shown in Figure 12. By eliminating every other isotherm in the database, the distribution changes, the first peak is reduced in height and becomes broader obviously due to the less expanse database. A third experiment was conducted with the original database of 63 local isotherms with a pore step size of 0.1nm, but reduced to cover the range of H = 0.6 nm to H = 5 nm. PSD(3) obtained is identical with PSD(1) implying that the contribution from the pores greater than H = 5 nm in width is negligible. In the previous study carried out by Lastoskie et al.[13] the PSD of AX21 carbon was also evaluated under similar conditions. A database containing 33 isotherms was used with an unequal step size in pore width and covered the range of H = 0.6 nm to H = 35.7 nm. After adjusting a scaling difference in Lastoskie's work[13] the PSD(4) was obtained and it is also presented in Figure 12. This pattern is in a good agreement with PSD(2) obtained in this work. The height of the first peak is almost identical for PSD(2) and PSD(4) corresponding to the approximately same number of local isotherms in the database used. PSD(2) and PSD(4) patterns start at a similar pore size, however, the second one peaks earlier, probably due to the different number of pressure points of local isotherms used by Lastoskie[14] (about 1/3 of ours) and the unequal step in calculation.

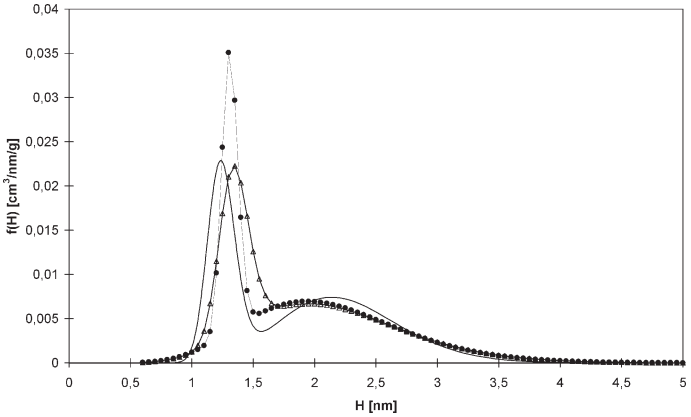

Fig. 12– *PSD(1) (●) for H = 0.6 nm to H = 100 nm and a step of 0.1 nm; PSD(3) (●) for H = 0.6 nm to H = 5 nm and a step of 0.1 nm (●); PSD(2) (Δ) for the step 0.2 nm and PSD(4) (solid line) according to Lastoskie*[14] *of AX21 from nitrogen adsorption*

In the previous calculations of PSDs two sets of α, β, γ parameters were used in solving the equation (7), i.e. the two-mode function. Alternatively a single set of parameters was also employed. Then the second peak of each distribution, which was evident when a bimodal function was used, was missing and the PSDs were all unimodal. RMSD values (10.1 and 10.2) were similar to those obtained for the two-mode experiment. It indicates that the number of inflection points in the experimental isotherms is a good indication of the number of modes to be used in solving for the most descriptive distribution.

Conclusion

Adsorption isotherms of nitrogen and argon on the surface of four and two microporous carbons were experimentally measured at 77K. Despite their significantly different adsorption properties nitrogen and argon formed two distinctive layers at comparable completion pressures on all the surfaces. This characteristic feature complied well with the major aim of the study to present a reliable theoretical method for evaluation of pore size distribution patterns of microporous carbons. Adsorption of both gases was also studied on the surface of non-microporous carbon Vulcan to predict potential parameters for the used adsorption model. Density functional theory was confirmed as a good method for calculation of local isotherms. The suggested algorithm for the pore size distribution analysis based on experimental isotherms and the theoretical database was shown to describe accurately the surface structure of different microporous carbons. Argon when used as an alternative surface probe under the same conditions revealed a higher sensitivity to ultra narrow pores compared with nitrogen. The extent of the database and the incremental increase in the physical pore width were identified as factors which directly influenced the calculated PSD patterns. It was shown that the resolution of the pore widths in the database does effect the shape of the PSD and that a step of 0.1nm is required to attain an accurate description of the surface.

ACKNOWLEDGEMENT

Authors wish to thank to Prof. Nick Quirke, Head of the Structural and Computational Chemistry Group, Department of Chemistry, Imperial College of Science, Technology and Medicine in London, for his continuous support, kind help and encouragement. We also thank to Steve Tennison for supplying AX21, and SJS thanks to Coulter-Beckmann Ltd., UK, for funding her studentship.

List of symbols

$\phi_{ff}(r)$ – Lennard-Jones (12–6) pair potential
r – separation distance between two fluid atoms
ε_{ff}, σ_{ff} – fitted parameters for the bulk adsorbate well-depth and molecular diameter
$\phi_{sf}(z)$ – Steele (10–4–3) potential.
z – distance from the graphite surface
σ_{sf} – effective adsorbate-adsorbent (carbon) intermolecular diameter
D – separation between graphite layers
ρ_s – number of carbon atoms per unit volume in graphite
ε_{sf} – parameter for the adsorbate-carbon interaction potential well-depth
$N(P)$ – experimental isotherm
$\rho(P,H)$ – local isotherm calculated
m – number of modes in the distribution
H – pore width
H_{phys} – physical pore width
α_i, β_i *and* γ_i – adjustable parameters
E – mean square error per a fitted point
n_P – number of experimental points
n_H – total number of pore widths

References:

1. *Soffel, R. W.*, Carbon and Artificial Graphite – a chapter in Kirk-Othmer Encyclopedia of Chemical Technology, Volume 4., p. 336., John Wiley&Sons, New York 1978.
2. *Schlogl, R.*, Carbons – a chapter in Handbook of Heterogeneous Catalysis, Volume 1, ed. by *Ertl, G., Knzinger, H.* and *Weitkamp, J.*, p.138., J. VCH Publishers, Weinheim 1997.
3. *Weissermel, K. and Arpe, H. J.*, Industriele Organische Chemie, p. 165., VCH Weinhem 1978.

4. *Thomas, J. M. and Thomas, W. J.*, Principles and Practise of Heterogeneous Catalysis, VCH, Weinheim, 1997.
5. *Olivier, J. P.*, J. Porous Materials **2** (1995) 9.
6. *McEnaney, B.*, *Mays, T. J.* and *Causton, P. D.*, Langmuir **3** (1987) 695.
7. *Maddox, M. W., Quirke, N. and Gubbins, K. E.*, Mol. Simulation **19** (1997) 267.
8. *Tan, Z. and Gubbins, K. E.*, J. Phys. Chem. **96** (1992) 845.
9. *Turner, A. R. and Quirke, N.*, Carbon **36** (1998) 1439.
10. *Lozovik, Y. E., Popov, A. M. and Letokhov, V. S.*, J. Phys. Chem. **99** (1995) 13480.
11. *Walton, J. P. and Quire, N.*, Molecular Simulatin **2** (1989) 361.
12. *Kluson, P., Scaife, S. J. and Quirke, N.*, Separation and Purification Technology **20** (2000) 15.
13. *Lastoskie, Ch., Gubbins, K. E. and Quirke, N.*, Langmuir **9** (1993) 2693.
14. *Cracknell, R. F., Nicholson, D. and Quirke, N.*, Mol. Sim. **13** (1994) 161.
15. *Cracknell, R. F., Nicholson, D. and Quirke, N.*, Mol. Phys. **80** (1993) 185.
16. *Gusev, V. Yu., O'Brien, A. O.*, Langmuir **14** (1995) 6328.
17. *Richter, E., Schütz, W., Myers, A. L.*, Chem. Eng. Sci. **44** (1989) 1609.
18. *Cracknell, R. F., Nicholson, D.*, Adsorption **1** (1995) 7.
19. *Nicholson, D., Gubbins, K. E.*, J. Chem. Phys. **104** (1996) 8126.
20. *Dune, J., Myers, A. L.*, Chem. Eng. Sci. **49** (1994) 2941.
21. *Finn, J. E., Monson, P. A.*, Molecular Physics **75** (1991) 661.
22. *Ramalho, J. P. and Smirnov, G. V.*, Langmuir **16** (2000) 1918.
23. *Ghassemzadeh, J., Xu, L. and Sahimi, M.*, J. Phys.Chem. B **104** (2000) 3896.
24. *Sing, K. S. W. and Rouquerol, J.*, Characterization of Solids – a chapter in Handbook of Heterogeneous Catalysis, ed. by Ertl G., Knzinger H. and Weitkamp J., p. 427., Volume 2,VCH Publishers, Weinheim 1997.
25. *Quirke, N. and Tennison, S. R.*, Carbon **34** (1996) 1281.
26. *Aukett, P. N., Quirke, N., Riddiford, S. and Tennison, S. R.*, Carbon **30** (1992) 913.
27. *McEnaney, B.*, Carbon **26** (1986) 267.
28. *Marsh, H. and Rand, B. J.*, Colloid. and Interface Sci. **33** (1970) 101.
29. *Efremov, D. K. and Fenelonov, V. B.*, React. Kinet. Catal. Lett. **52** (1994) 413.
30. *Medek, J.*, Fuel **53** (1977) 131.
31. *Nakashima, M., Shimada, S., Inagaki, M. and Centeno, T. A.*, Carbon **33** (1995) 1301.
32. *Evans, R.*, J. Phys. Cond. Matter **2** (1990) 8989.
33. *Tarazona, P., Evans, R.*, Molec. Phys. **52** (1984) 847.
34. *Kierlik, E., Rosinberg, M.*, Mol. Phys. **75** (1992) 1435.
35. *Kierlik, E, Rosinberg, M.*, Phys. Rev. A **44** (1991) 5025.
36. *Shigeta, T., Yoneya, J. and Nitta, T.*, Molecular Simulation **16** (1996) 291.
37. *Scaife, S. J., Kluson, P. and Quirke, N.*, J. Phys. Chem. B **104** (2000) 313.
38. Laboratory of Government Chemist – EU certification documents for IUPAC surface area standards Vulcan and Sterling, Teddington 1997.
39. *Kaneko, K., Cracknell, R.F. and Nicholson, D.*, Langmuir **10** (1994) 4606.
40. *Sing, K. S. W.*, Pure Appl. Chem. **57** (1985) 603.
41. *Kierlik, E., Rosinberg, M., Finn, J. and Monson, P. A.*, Mol. Phys. **75** (1992) 1435.
42. *Rigby, M., Smith, E. B., Wakeham, W. A. and Maitland, G. C.*, in The Forces Between Molecules, Oxford Science Publications, Oxford 1986.
43. *Gray, C. G. and Gubbins, K. E.*, in Theory of Molecular Fluids, Oxford Science Publications, Oxford 1984.
44. *Allen, M. P. and Tildesley, D. J.*, Computer Simulation of Liquids, Oxford Science Publications, Oxford 1987.
45. *Sirkar, S. J.*, Colloid. Interface Sci. **101** (1984) 452.
46. *Maglara, E., Pullen, A., Sullivan, D. and Conner, W. C.*, Langmuir **10** (1994) 4167.
47. *Banares-Munoz, M. A., Flores Gonzales, L. V. and Martin Llorenta, J. M.*, Carbon **25** (1987) 603.
48. *Gilgen, R., Kleinrahm, R. and Wagner, W.*, J.Chem.Thermodynamics **26** (1994) 399.
49. *Kluson, P. and Scaife, S. J.*: J. Porous Materials, submitted.